Joint Activity and Attenuation Reconstruction of Listmode TOF-PET data

Ahmadreza Rezaei[1], Matthew Bickell[1], Roger Fulton[2], Johan Nuyts[1]

***Abstract*—Different methods have been proposed for simultaneous reconstruction of activity and attenuation from TOF-PET sinogram data. In this work we present the listmode maximum likelihood activity and attenuation reconstruction (MLAA) and the listmode maximum likelihood attenuation correction factors (MLACF) algorithms building on their established sinogram implementation. Our listmode MLAA differs from a recently proposed listmode algorithm by incorporating the maximum likelihood transmission reconstruction (MLTR) algorithm in MLAA. The listmode MLTR algorithm has some similarity to the listmode image based reconstruction algorithm (ISRA), since it reconstructs the image from the backprojection of the acquired data. We investigate the reconstruction results on a scan of the NEMA IEC body phantom.**

I. Introduction

It has been shown that the information in time-of-flight (TOF) positron emission tomography (PET) emission data is rich enough to solve the long-standing problem of activity and attenuation cross-talk [1], [2]. The majority of algorithms that have been developed for joint reconstruction of activity and attenuation require an initial histogramming of the listmode data into a sinogram. In an attempt to directly use the listmode data in the joint reconstruction framework, Mollet et al. [3] proposed a method that combines the listmode TOF-MLEM reconstruction of the activity image [4], [5] with an MLTR-like algorithm for the reconstruction of the attenuation image.

In the same spirit, we extend the previously developed sinogram implementation of the MLAA algorithm to handle listmode data. In reconstruction from transmission data which are subject to Poisson noise, the backprojection of the data is a sufficient statistic. Because of this, MLTR reconstructs the image from the backprojection of the transmission data. This makes it similar to ISRA [6], which was developed for emission data and for which a listmode implementation has been proposed [7]. Furthermore, we extend the maximum likelihood attenuation correction factors (MLACF) algorithm to handle listmode data. We find that although the attenuation correction factors (ACFs) are not computed explicitly, they are corrected for during reconstructions. The results of the listmode transmission reconstruction algorithm are shown for the NEMA IEC body phantom and then the listmode joint reconstructions are compared to the sinogram reconstructions of the TOF-PET emission data.

This research is supported by a research grant (GOA) from K.U.Leuven, FWO project G027514N and by Australian Research Council Discovery Grant DP110104604.

[1]Nuclear Medicine, K.U.Leuven, B-3000 Leuven, Belgium. [2]Brain & Mind Research Institute and the Faculty of Health Sciences, University of Sydney, Australia.

II. Methods

The listmode-MLAA algorithm uses an interleaved updating of the activity/attenuation reconstruction while keeping the attenuation/activity reconstruction fixed. The algorithm can be written as follows:

$$\forall i: \quad a_i^{(n)} = e^{-\sum_j l_{ij}\mu_j^{(n)}} \tag{1}$$

$$\forall j: \quad \lambda_j^{(n+1)} = \frac{\lambda_j^{(n)}}{\sum_i c_{ij} a_i^{(n)}} \sum_m c_{i_m j t_m} \frac{1}{\sum_\xi c_{i_m \xi t_m} \lambda_\xi^{(n)}} \tag{2}$$

$$\forall i: \quad \bar{y}_i^{(n+1)} = a_i^{(n)} \sum_j c_{ij} \lambda_j^{(n+1)} \tag{3}$$

$$\forall j: \quad \mu_j^{(n+1)} = \mu_j^{(n)} - \frac{\sum_m l_{i_m j} - \sum_i l_{ij} \bar{y}_i^{(n+1)}}{\sum_i l_{ij} \bar{y}_i^{(n+1)} \sum_\xi l_{i\xi}} \tag{4}$$

where μ and λ are the attenuation and activity reconstructions, the superscript denotes the iteration number, l_{ij} is the intersection length of LOR i and voxel j and a_i is the attenuation correction factor along LOR i. c_{ij} (c_{ijt}) is the sensitivity of voxel j to LOR i (and TOF-bin t), i_m and t_m are the LOR and TOF-bin corresponding to event m, and $\bar{y}_i$ is the expected non-TOF counts along LOR i. Note that the range of the sums over index i are over all possible LORs whereas the sums over i_m are over all the list mode events.

The algorithm was accelerated using ordered subsets as well as applying multiple attenuation updates for each update of activity. For summations involving the measurements, the events in a subset were chosen by taking every kth event, where k is the number of subsets. For the summation over all possible LORs, a set of r LORs were sub-sampled from the list of all possible LORs, where r is the number of listmode events in the emission subset. Furthermore, similar to ISRA we took advantage of back-projecting the measured counts once and re-using this back-projection in (4) during the iterations.

In contrast to MLAA, the MLACF algorithm uses an interleaved updating of the attenuation correction factors (ACFs) together with the activity reconstruction. When the additive contributions of randoms and/or scatter are ignored, MLACF gives an immediate update of the ACFs [8]. The listmode extension of this algorithm can be written as follows:

$$\forall i_m: \quad p_{i_m}^{(n)} = \sum_\xi c_{i_m \xi} \lambda_\xi^{(n)} \tag{5}$$

$$\forall j: \quad \lambda_j^{(n+1)} = \frac{\lambda_j^{(n)}}{\sum_m c_{i_m j} \frac{1}{p_{i_m}^{(n)}}} \sum_m c_{i_m j t_m} \frac{1}{p_{i_m t_m}^{(n)}} \tag{6}$$

where $p_{i_m}^{(n)}$ is the non-TOF projection of the activity reconstruction (and similarly $p_{i_m t_m}$ is the TOF projection at listmode event (i_m, t_m)). Note that the listmode MLACF algorithm does not explicitly estimate the ACF values along all measured LORs; however, the effects of the ACFs are corrected for during reconstructions through the estimation of their back-projection commonly referred to as the sensitivity image. Furthermore, the listmode MLACF reconstruction benefits from using two matched back-projections compared to the listmode MLEM and MLTR algorithms where the reconstructions involve back-projections of the measured events as well as the back-projections of all possible LORs.

III. Experiment Design

The NEMA IEC body phantom was filled with 200 MBq of ^{18}F-FDG, and scanned with the Siemens Biograph mCT for 1 hour. The emission data were acquired 3 hours post-injection. Only a subset of the TOF-PET emission data corresponding to the first 10 minutes was used in the reconstruction. An initial MLEM activity reconstruction with CT-based attenuation correction was obtained and used to produce a blank scan to test the listmode transmission reconstruction algorithm. Since we wanted to compare the results with the sinogram reconstructions, the 64-bit listmode events were mashed with the typical sinogram mashing to give 32-bit listmode event data. Activity and attenuation reconstructions were then obtained from the 32-bit listmode data using the listmode implementations of MLAA and MLACF. The listmode data were subsequently histogrammed to create the TOF-PET emission sinogram and the listmode reconstructions were compared to the reconstructions of the sinogram implementation of MLAA and MLACF. The TOF-PET emission sinogram consisted of 400 detectors, 168 angles, a total of 621 planes and 13 TOF-bins of 312 ps resolution. The effective TOF resolution of the system was 580 ps. In both implementations, the additive scatter/randoms contribution was ignored.

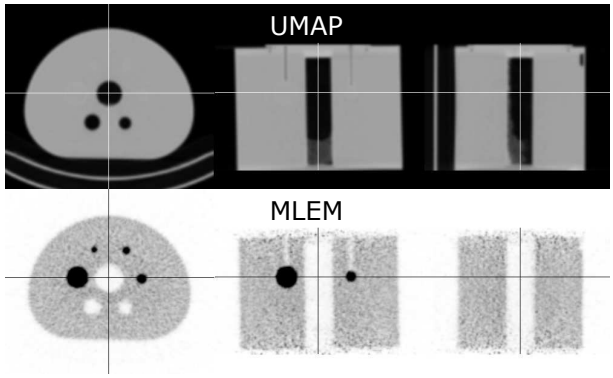

Fig. 1. CT-based attenuation image of the NEMA IEC phantom (top) and the TOF-MLEM activity reconstruction (bottom) used as a blank scan which is required for the MLTR algorithm. The activity reconstruction is post-smoothed with a Gaussian of 3 mm FWHM.

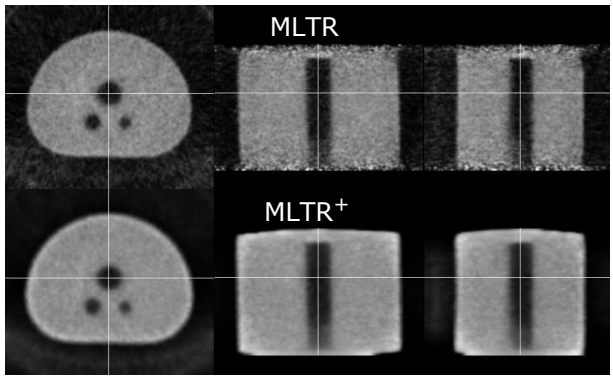

Fig. 2. Listmode MLTR attenuation reconstructions using the TOF-MLEM reconstruction (Fig. 1 - bottom) as a blank scan. The reconstructions are obtained without a smoothing prior (top) and with the relative difference prior (bottom) to suppress the background attenuation during iterations. The attenuation reconstructions are post-smoothed with a Gaussian of 3 mm FWHM.

IV. Results

Figure 2 shows the listmode MLTR attenuation reconstructions of the data, when the TOF-MLEM activity reconstruction (shown in figure 1) was used as the known activity. The MLTR$^+$ attenuation reconstruction of figure 2 was regularized by the relative difference prior [9] during reconstruction. In our experience, little effort was needed to limit the attenuation build-up in the background region of the image (region with no activity present).

Figures 3 and 4 show the listmode and sinogram reconstructions of MLAA and MLACF for the NEMA IEC body phantom, respectively. The total MLEM counts were used to scale the joint activity reconstructions, and as in the case of MLTR, for MLAA no extra measures were taken to limit the attenuation build-up in the background region. Although the activity and attenuation images look cross-talk free, some differences are still observed especially close to edge of the phantom (the region with limited TOF sampling along some LORs). In both (listmode and sinogram) attenuation reconstructions, some excess attenuation was put outside the support of the activity which is most likely because the scatter/randoms were not corrected for. A visual comparison of reconstructions of 64-bit listmode data (the results not shown here) revealed a slight improvement in the reconstructions mostly visible at high gradients of the activity reconstruction. A more comprehensive comparison between the reconstructions is underway.

Although the attenuation correction factors cannot be explicitly computed with listmode data, the activity reconstructions of the listmode and sinogram MLACF reconstructions (figures 3 and 4, respectively) are visually similar. Furthermore, in the case of reconstructions of motion-corrected listmode events, the computation of a time-averaged sensitivity image can become challenging and computationally demanding. Since a back-projection of all possible LORs does not appear in the listmode MLACF update (eqn. (6)) as opposed to the update of MLEM (eqn. (2)), the algorithm benefits by automatically incorporating the time-averaged sensitivity image during reconstruction. We intend to investigate this property in more detail in the future.

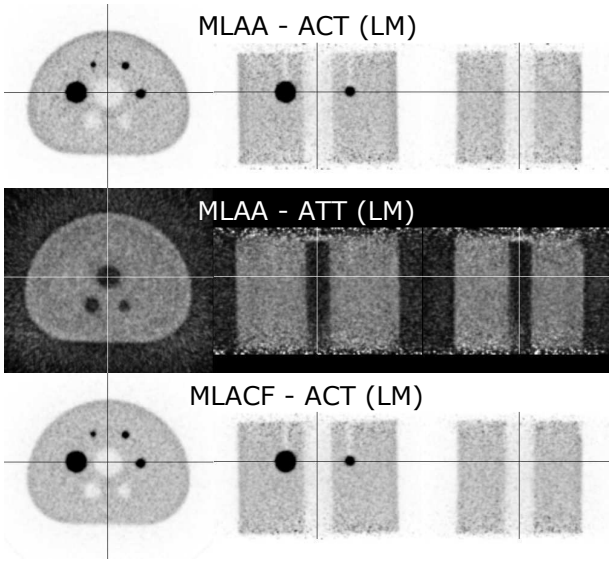

Fig. 3. Listmode activity and attenuation reconstructions of MLAA (top and center) and the MLACF activity reconstruction (bottom).

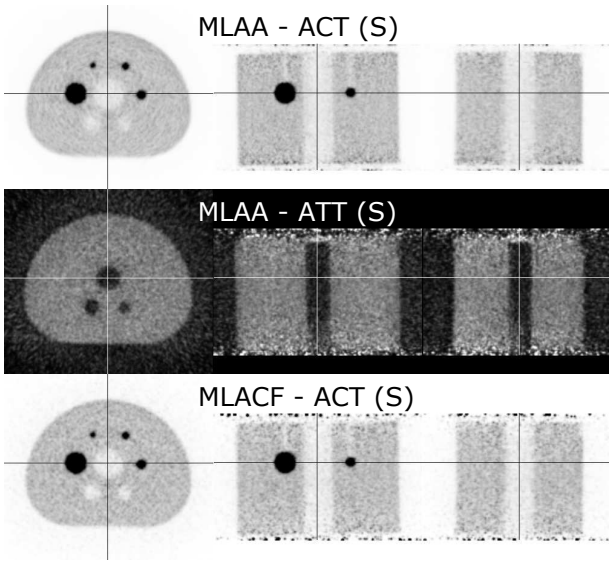

Fig. 4. Sinogram activity and attenuation reconstructions of MLAA (top and center) and the MLACF activity reconstruction (bottom).

V. Conclusion

The MLAA and MLACF reconstruction algorithms were originally developed for reconstructions of activity and attenuation images using the TOF-PET sinogram of the emission data. In this study, we present the listmode version of these algorithms for the case of no randoms and/or scatter contribution. The listmode and sinogram reconstructions of a 10 minute NEMA scan seem visually comparable, however further investigation is required to explain some of the differences observed especially at the edge of the phantom. Our results currently suggest that the typical mashing of the listmode data required to obtain the emission sinogram does not greatly influence the activity and attenuation reconstructions.

VI. Acknowledgments

The authors would like to thank Jung-Ha Kim for data collection as well as Georgios Angelis, John Gillam and Will Ryder for the very insightful discussions.

References

[1] M. Defrise, A. Rezaei, and J. Nuyts, "Time-of-flight PET data determine the attenuation sinogram up to a constant." *Phys. Med. Biol.*, vol. 57, no. 4, pp. 885–99, Feb. 2012.

[2] A. Rezaei, M. Defrise, G. Bal, C. Michel, M. Conti, C. Watson, and J. Nuyts, "Simultaneous reconstruction of activity and attenuation in time-of-flight PET." *IEEE Trans. Med. Imaging*, vol. 31, no. 12, pp. 2224–33, Dec. 2012.

[3] P. Mollet and S. Vandenberghe, "Comparison of transmission- and emission-based attenuation correction for TOF-PET / MRI," in *2014 IEEE Nucl. Sci. Symp. Med. Imaging Conf. (2014 NSS/MIC)*, 2014, pp. 1–5.

[4] L. Parra and H. H. Barrett, "List-mode likelihood: EM algorithm and image quality estimation demonstrated on 2-D PET." *IEEE Trans. Med. Imaging*, vol. 17, no. 2, pp. 228–35, Apr. 1998.

[5] a. Rahmim, P. Bloomfield, S. Houle, M. Lenox, C. Michel, K. Buckley, T. Ruth, and V. Sossi, "Motion compensation in histogram-mode and list-mode EM reconstructions: beyond the event-driven approach," *IEEE Trans. Nucl. Sci.*, vol. 51, no. 5, pp. 2588–2596, Oct. 2004.

[6] A. R. De Pierro and I. Ax, "On the Convergence of the Iterative Image Space Reconstruction Algorithm for Volume ECT." *IEEE Trans. Med. Imaging*, vol. 6, no. 2, pp. 174–175, 1987.

[7] M. G. Bickell, J. Gillam, R. Fulton, and J. Nuyts, "Spatially Variant Resolution Modelling Using Redistributed Lines-of-Response and the Image Space Reconstruction Algorithm," in *2014 IEEE Nucl. Sci. Symp. Med. Imaging Conf. (2014 NSS/MIC) IEEE Nucl. Sci. Symp. Conf. Rec.*, 2014.

[8] M. Defrise, A. Rezaei, and J. Nuyts, "Transmission-less attenuation correction in time-of-flight PET: analysis of a discrete iterative algorithm." *Phys. Med. Biol.*, vol. 59, no. 4, pp. 1073–95, Feb. 2014.

[9] J. Nuyts, D. Beque, P. Dupont, and L. Mortelmans, "A concave prior penalizing relative differences for maximum-a-posteriori reconstruction in emission tomography," *IEEE Trans. Nucl. Sci.*, vol. 49, no. 1, pp. 56–60, Feb. 2002.